Journal of Statistical Physics, Vol. 105, Nos. 3/4, November 2001 (© 2001)

Non-Equilibrium Behaviour in Unidirectionally Coupled Map Lattices

Frank Schmüser[1] **and Wolfram Just**[2,3]

Received October 30, 2000; revised June 12, 2001

A spatially one dimensional coupled map lattice with a local and unidirectional coupling is introduced. This model is studied analytically by a perturbation theory that is valid for small coupling strength. In parameter space three phases with different ergodic behaviour are observed. Via coarse graining the deterministic model is mapped to a stochastic spin model that can be described by a master equation. Because of the anisotropic coupling non-equilibrium behaviour is found on the coarse grained level. However, the stationary statistical properties of the spin dynamics can still be described with a nearest neighbour Ising model whereby the ordering is predominantly antiferromagnetic.

KEY WORDS: Coupled maps; kinetic Ising model; chaos; nonequilibrium phase transition.

1. INTRODUCTION

Non-equilibrium physics in general and transport phenomena in particular are one of the most challenging fields in modern theoretical physics. Unfortunately, there does not exist a general framework for the investigation of non-equilibrium features. Thus, in the whole subject a variety of methods is discussed, ranging from full scale microscopic equations of motion, driven master equations, stochastic models, hydrodynamic descriptions, cellular automata and coupled map lattices (see, e.g., refs. 1–3).

[1] Department of Physics, Virginia Tech, Blacksburg, Virginia 24061-0435; e-mail: schmuser@kanga.phys.vt.edu

[2] School of Mathematical Sciences, Queen Mary & Westfield College, Mile End Road, London E1 4NS, United Kingdom; e-mail: W.Just@qmw.ac.uk

[3] Present address: Institut für Physik, TU-Chemnitz, D-09107 Chemnitz, Germany.

0022-4715/01/1100-0525$19.50/0

A certain boost was caused by developments in nonlinear dynamics, in particular by the understanding of chaotic motion. Thus, an overlap between dynamical systems theory and statistical mechanics has occurred even from the physics point of view.

Coupled map lattices (CMLs) have been introduced as a widely studied model class for spatio-temporal chaos[4, 5] at the end of the eighties. In such models local chaos is generated by a chaotic map that is placed on each site of a simple lattice. Spatial aspects are introduced by coupling these local units, and special emphasis is on the limit of large lattice size where the dynamics becomes high dimensional. The application of methods that were developed in the context of equilibrium statistical physics have proven to be fruitful for the study of high dimensional chaos in CMLs. In particular coarse graining is a common tool. In rigorous approaches coarse graining is performed by suitable partitions of the phase space and there are results for particular coupled map lattices available (cf. refs. 6 and 7). Unfortunately, so far such rigorous schemes are limited to the perturbative regime of hyperbolic CMLs and are technically extremely difficult to apply.

It is an important question from a theoretical point of view whether a coupled map lattice finally leads to an equilibrium or a non-equilibrium statistical mechanics, i.e., whether the condition of detailed balance holds. In a recent publication the authors investigated the relation between CMLs and spin models by means of an analytical perturbation theory.[8] In this CML the coupling of a lattice site to its two neighbours was symmetric, and equilibrium behaviour was found for the spin dynamics. In this article we establish a similar link between a deterministic CML dynamics and a stochastic spin dynamics for a strongly asymmetric coupling.

We should mention that the main focus of the present contribution is on principal aspects of dynamics in spatially extended systems. There does not exist a deep relation between coupled map lattices and real experiments on a quantitative basis. However, we expect that some features of our model are typical and can even be observed in experiments. Transport properties subjected to strong external fields, i.e., transport under strong nonequilibrium conditions, is already one of the meanwhile classical topics in statistical mechanics (cf., e.g., ref. 2). Even beyond traditional fields of physics such nonequilibrium phenomena become increasingly important. Natural applications arise in a biochemical context, like, e.g., molecular motors and the understanding of the associated transport phenomena.[9] Whether models which deduce macroscopic net currents from the interplay between nonequilibrium noise and asymmetric potentials, i.e., so called ratchets,[10] really describe the underlying mechanisms seems to be still under discussion. However, the situation shows, that even rough modelling of key features may shed some light on experimentally relevant features.

Thus in a wider perspective our model system may contribute to such fields as well.

We now outline the organisation of the article. Section 2 introduces the CML and its perturbative regime. In Section 3 results of the perturbative treatment of the CML are presented, among them the bifurcation scenario. The method of investigation is the same as the one used in ref. 8. The coarse graining of the CML that gives rise to a corresponding stochastic spin dynamics is carried through in Section 4. With the help of these tools we study the ergodic properties in the various regions of the bifurcation diagram in Section 5, both for the deterministic CML and the corresponding spin dynamics. An order–disorder phase transition of antiferromagnetic character is found. The non-equilibrium behaviour that is present on the coarse grained level is studied in detail in Section 6. In Section 7 we show how to cope with the case of very strong coupling. Finally, the results of this article are summarised in Section 8. To keep the technical details in the main part at a minimum, the article contains three appendixes. These appendixes contain derivations of important results for the CML and its stochastic description.

2. THE MODEL

The single site map f_δ of the CML is a deformed antisymmetric tent map that is linear on three subintervals of $[-1, 1]$ (cf. Fig. 1)

$$f_\delta(x) := \begin{cases} -2 - x/a & \text{if} \quad x \in [-1, -a] \\ x/a & \text{if} \quad x \in (-a, a) \\ 2 - x/a & \text{if} \quad x \in [a, 1] \end{cases} \tag{1}$$

with $a := 1/(2-\delta)$. The introduction of a in Eq. (1) ensures that the modulus of the derivative of f_δ is constant on the whole interval. Since $f_\delta(1) = \delta$, the parameter δ determines whether transitions between the intervals $J(-1) := [-1, 0]$ and $J(+1) := [0, 1]$ are possible. Figure 1

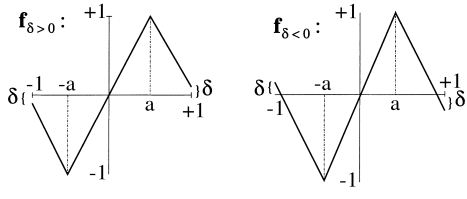

Fig. 1. The deformed antisymmetric tent map f_δ.

shows the function f_δ for small positive and negative δ. At $\delta = 0$ the map f_δ undergoes a symmetry breaking bifurcation, i.e., for $\delta \geqslant 0$ the single site map has two coexisting attractors, the intervals $[-1, \delta]$ and $[\delta, 1]$, whereas for $\delta < 0$ only one attractor, the interval $[-1, 1]$, is present. Later we will identify the positive interval $[0, 1]$ with spin $+1$, the negative interval $[-1, 0]$ with spin -1. The single site map f_δ has also been used in ref. 8.

The CML that is studied in this article is defined on a one dimensional lattice (chain) of length N. The coupling is unidirectional or one-way: a lattice site i is coupled only to its right neighbour $i+1$

$$\mathbf{T}_{\epsilon,\delta}: [-1, +1]^N \to [-1, +1]^N,$$
$$x_i^{t+1} = [\mathbf{T}_{\epsilon,\delta}(\mathbf{x})]_i := (1-\epsilon)\, f_\delta(x_i^t) + \epsilon f_\delta(x_{i+1}^t), \qquad i = 1, 2, \ldots, N. \quad (2)$$

The index $t \in \mathbb{N}$ is the time index. The CML $\mathbf{T}_{\epsilon,\delta}$ contains two parameters, the coupling strength ϵ and the deformation δ of the single site map f_δ. The coupling strength can be chosen between 0 and 1. We impose periodic boundary conditions in the CML ($x_{N+1}^t = x_1^t$). Therefore, translation invariance on the one dimensional lattice holds. Because of the single site map f_δ and the form of the coupling in Eq. (2) the CML $\mathbf{T}_{\epsilon,\delta}$ also has the symmetry $T_{\epsilon,\delta}(-x) = -T_{\epsilon,\delta}(x)$.

Our main interest in this article is the ergodic behaviour of the CML $\mathbf{T}_{\epsilon,\delta}$. We would like to know how many and which attractors are present for given parameters ϵ, δ. Unfortunately, our analytic approach is not applicable for general parameters, but restricted to the regions of small and large coupling, i.e., $\epsilon \ll 1$ and $(1-\epsilon) \ll 1$. We also assume a small deformation $|\delta| \ll 1$. We will see that the ergodic behaviour of the CML already is quite rich in these small subregions of parameter space. The case of very large coupling ($\epsilon \approx 1$) will be dealt with in Section 7, so that we start with considering the perturbative region $\epsilon, |\delta| \ll 1$.

In order to set up a perturbation theory, we first look at the CML with $\epsilon = \delta = 0$ that can be solved trivially. The non–deformed antisymmetric tent map $f_{\delta=0}$ has the two attractors $J(-1) := [-1, 0]$ and $J(+1) := [0, 1]$. For N lattice sites there are 2^N coexisting attractors, each one being an N dimensional cube of edge length one

$$I_\alpha := J(\alpha_1) \times J(\alpha_2) \times \cdots \times J(\alpha_N). \quad (3)$$

We distinguish these cubes I_α by an N dimensional index vector $\boldsymbol{\alpha} = (\alpha_1, \alpha_2, \ldots, \alpha_N)$ where $\alpha_i \in \{-1, +1\}$. These cubes will be important building blocks of the perturbation theory and the starting point of a coarse grained description of the CML $\mathbf{T}_{\epsilon,\delta}$.

3. TRANSITIONS AND BIFURCATIONS

In this section we summarise the dynamics of the CML in the perturbative regime ($\epsilon, |\delta| \ll 1$). First, we note that for a CML orbit $\{\mathbf{x}^t,\ t = 0, 1, 2, \ldots\}$ each coordinate x_i^t stays a rather long time in the interval $J(\alpha_i) \in \{J(+1), J(-1)\}$, before it possibly enters the other interval $J(-\alpha_i)$ via a change of sign. Such a sign change will be called a transition in the following. Here both the positive and negative values of the coordinate should have a magnitude $\mathcal{O}(1)$, so that both intervals are really visited by the CML coordinate.

Looking at all coordinates, we can characterise the CML dynamics by successive changes of cube $I_\alpha \to I_\beta$. For not too large lattices ($N \ll 1/\epsilon$) at most one transition takes place per iteration step in the perturbative regime of the CML. For large lattices simultaneous transitions at different sites occur in the change of cube $I_\alpha \to I_\beta$. However, the average distance between the involved lattice sites is rather large.

In the perturbative regime any attractor of the CML $\mathbf{T}_{\epsilon,\delta}$ is a union of cubes I_α neglecting sets with volume $\mathcal{O}(\epsilon, \delta)$. An attractor is a minimal union of cubes such that this union can not be left via a transition of a coordinate x_i^t. Thus, the allowed transitions for given parameters ϵ, δ determine the attractors of the CML for this choice of parameters.

In the spirit of perturbation theory we can confine ourselves to the analysis of dominant transitions that we now define. In a dominant transition the two neighbouring coordinates x_{i-1}^t and x_{i+1}^t stay in their respective interval, if the coordinate x_i^t changes its sign at time t_0. Transitions in which two or more neighbouring coordinates change sign at the same time are suppressed in perturbation theory by an additional factor $\mathcal{O}(\epsilon, \delta)$.

The decisive simplification of perturbation theory for the unidirectional CML $\mathbf{T}_{\epsilon,\delta}$ is that only the coordinate x_i^t itself and its neighbouring one x_{i+1}^t have to be considered for a transition. For, according to Eq. (2) the CML couples only the neighbour coordinate x_{i+1}^t to the coordinate x_i^t during one iteration. In the perturbative regime the dominant influence of the neighbour coordinate also persists for the finite amount of time that is needed for a transition, since the influence of lattice sites further away is suppressed by a factor of $\mathcal{O}(\epsilon^2)$. Thus the remaining $(N-2)$ coordinates only play a spectator role for the transition. Therefore, one can study all dominant transitions in a CML with only two lattice sites. A transition can be denoted by $\alpha_i\alpha_{i+1} \to -\alpha_i\alpha_{i+1}$. Because of the symmetries of the CML $\mathbf{T}_{\epsilon,\delta}$ we have two types of transitions:

Type (a): the two indices α_i and α_{i+1} are equal,

$$+1+1 \to -1+1 \qquad \text{or} \qquad -1-1 \to +1-1. \tag{4}$$

Type (b): α_i and α_{i+1} differ,

$$-1+1 \to +1+1 \qquad \text{or} \qquad +1-1 \to -1-1. \tag{5}$$

For each transition type there is a critical value $\delta_{\text{crit}}(\epsilon)$ such that for fixed ϵ a transition type becomes only possible, if the deformation parameter δ is smaller than this critical value. We obtain for the critical values $\delta_{\text{crit}}(\epsilon)$

$$\text{type (a):} \quad \delta_a = 0, \qquad \text{type (b):} \quad \delta_b = -\frac{4\epsilon}{3}. \tag{6}$$

The calculation of these critical values necessitates rather involved geometric constructions in the reduced two dimensional phase space in which the relevant dynamics for the transition takes place. Hence, these calculations are deferred to Appendix A. As we are doing perturbation theory, we expect corrections to the critical values in Eq. (6) of order $\mathcal{O}(\epsilon^2)$.

Equation (6) determines the global bifurcations of the CML $\mathbf{T}_{\epsilon,\delta}$. A bifurcation occurs, if a transition type becomes allowed or forbidden by a change of parameters. This is the case, if for fixed coupling constant ϵ the deformation parameter δ crosses a bifurcation line $\delta_{\text{crit}}(\epsilon)$. The bifurcation diagram of the CML in the perturbative regime is shown in Fig. 2. The two bifurcation lines separate three regions with different ergodic behaviour. The ergodic dynamics in the various regions will be discussed in Section 5, after having introduced a coarse graining of the CML.

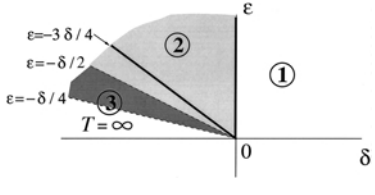

Fig. 2. Diagrammatic view of the bifurcation diagram for the unidirectional CML $\mathbf{T}_{\epsilon,\delta}$. The three parameter regions of Section 5 are labeled by numbers. Gray shading indicates the type of coupling in the corresponding kinetic Ising model, antiferromagnetic (light) or ferromagnetic (dark). There is also a region where the temperature is ∞.

4. COARSE GRAINING OF THE CML

In a coarse grained perspective one passes from orbits $\{\mathbf{x}^t, t = 0, 1, 2,\ldots\}$ in phase space to symbol or spin chains $\{\boldsymbol{\alpha}^t, t = 0, 1, 2,\ldots\}$. We introduce two possible spin states per lattice site

$$\alpha_i(t) := \begin{cases} +1, & \text{if } x_i^t \geqslant 0 \\ -1, & \text{if } x_i^t < 0. \end{cases} \tag{7}$$

Hence, if an orbit of the CML performs a cube change $I_\alpha \to I_\beta$, the state of the spin chain changes from $\boldsymbol{\alpha}$ to $\boldsymbol{\beta}$ via a spin flip. As explained in Section 3, a cube change $I_\alpha \to I_\beta$ consists of $k \ll N$ local transitions of CML coordinates x_i^t that occur at the same time. Hence a change of spin configuration $\boldsymbol{\alpha} \to \boldsymbol{\beta}$ is composed out of local spin flips $\alpha_i \to -\alpha_i$.

We seek for a quantitative description of the spin dynamics in terms of the spin states $\boldsymbol{\alpha}^t$ alone. This description has to be stochastic, since on the coarse grained level the information about the precise location of the CML trajectory has been lost. Hence we introduce a vector $\mathbf{p}(t)$ where a component $p_\alpha(t)$ gives the probability of spin configuration $\boldsymbol{\alpha}$ at time t. We make the following observations concerning the spin dynamics in the perturbative regime; more detailed considerations can be found in Appendix C.

1. A local spin flip $\alpha_i \to -\alpha_i$ in the spin configuration corresponds to a transition $\alpha_i\alpha_{i+1} \to -\alpha_i\alpha_{i+1}$ in the CML $\mathbf{T}_{\epsilon,\delta}$. As mentioned above, in the perturbative regime of the CML $\mathbf{T}_{\epsilon,\delta}$ only the coordinates x_i^t and x_{i+1}^t play a role for this transition. Both coordinates stay a rather long time in the square $J(\alpha_i) \times J(\alpha_{i+1})$, before the transition takes place. Since the CML dynamics is also highly chaotic and mixing, the memory of a preceding transition of one of the two coordinates x_i^t and x_{i+1}^t gets lost. Hence, in the perturbative regime a local spin flip $\alpha_i \to -\alpha_i$ is a Markov process of first order and can be described by a transition probability per time step $w^{(2)}(\alpha_i\,\alpha_{i+1} \to -\alpha_i\,\alpha_{i+1})$ that only depends on the spin states at lattice site i and $i+1$ before and after the spin flip. If a site i does not flip in the change of spin configuration $\boldsymbol{\alpha} \to \boldsymbol{\beta}$, we assign a probability $1 - w^{(2)}(\alpha_i\,\alpha_{i+1} \to -\alpha_i\,\alpha_{i+1})$ for this.

2. In Appendix C it is shown that two simultaneous spin flips $\alpha_i \to -\alpha_i$ and $\alpha_j \to -\alpha_j$ do not influence each other, if $|i-j| > 1$. As explained in Section 3, perturbatively dominant transitions obey this condition. Hence, simultaneous spin flips can be treated as statistically independent.

If we take these two points into account, the following master equation for the stochastic spin dynamics arises

$$p_{\alpha}(t+1) = p_{\alpha}(t) + \sum_{\beta \neq \alpha} [w(\boldsymbol{\alpha} \mid \boldsymbol{\beta}) \cdot p_{\beta}(t) - w(\boldsymbol{\beta} \mid \boldsymbol{\alpha}) \cdot p_{\alpha}(t)]. \tag{8}$$

Here the transition probability $w(\boldsymbol{\beta} \mid \boldsymbol{\alpha})$ per time step for the process $\boldsymbol{\alpha} \to \boldsymbol{\beta}$ is given as

$$\begin{aligned} w(\boldsymbol{\beta} \mid \boldsymbol{\alpha}) = \prod_{i=1}^{N} [& \delta_{-\beta_i, \alpha_i} w^{(2)}(\alpha_i \, \alpha_{i+1} \to -\alpha_i \, \alpha_{i+1}) \\ & + \delta_{\beta_i, \alpha_i} (1 - w^{(2)}(\alpha_i \, \alpha_{i+1} \to -\alpha_i \, \alpha_{i+1}))], \end{aligned} \tag{9}$$

where we have used the Kronecker symbol. Thus the transition probability $w(\boldsymbol{\beta} \mid \boldsymbol{\alpha})$ is a product of N local factors, each one only depending on the spin configuration at lattice sites i and $i+1$.

Let us finish this section with some remarks about the local spin flip probabilities $w^{(2)}(\alpha_i \, \alpha_{i+1} \to -\alpha_i \, \alpha_{i+1})$. This quantity can take on the two values w_a and w_b, depending on whether the spin flip is of type (a) or (b). As only the flipping spin α_i and its right neighbour α_{i+1} enter the expression $w^{(2)}(\alpha_i \, \alpha_{i+1} \to -\alpha_i \, \alpha_{i+1})$, the spin interaction is local and strongly asymmetric. This asymmetry is due to the one-way coupling in the CML $\mathbf{T}_{\epsilon, \delta}$ (cf. Eq. (2)). The spin flip probabilities w_a and w_b can be determined on a CML with only two lattice sites ($N = 2$). In Appendix A expressions for these quantities could be derived that describe the area of certain two dimensional sets in phase space (cf. Eqs. (A21) and (A26)). If δ is greater than the corresponding critical value in Eq. (6), the respective transition probability strictly vanishes, as these sets become empty then. Lowering δ the transition probabilities increase monotonically. It is possible to obtain simple formulas for w_a and w_b for special values of ϵ, δ (cf. Eqs. (A23) and (A27) of Appendix A). For large deformation $|\delta|$ we obtain the following results

$$\begin{aligned} w_a &= -\frac{\delta}{2} - \epsilon, \qquad \delta < -\frac{8\epsilon}{3}, \\ w_b &= -\frac{\delta}{2} - \epsilon, \qquad \delta < -4\epsilon. \end{aligned} \tag{10}$$

5. THE ERGODIC DYNAMICS OF THE CML

We will now discuss the ergodic dynamics of the CML $\mathbf{T}_{\epsilon,\delta}$ and the corresponding spin dynamics on the coarse grained level in the various regions of parameter space (cf. the bifurcation diagram in Fig. 2).

Region 1 ($\delta > 0$). In this region no transitions take place, and every cube contains an attractor, so there are 2^N coexisting attractors.

Region 2 ($-4\epsilon/3 < \delta < 0$). In this region only transitions/spin flips of type (a) are possible ($w_a > 0$, $w_b = 0$). For the discussion of the spin dynamics the introduction of defects in the spin chains $\boldsymbol{\alpha}$ proves to be very useful. We introduce defects on the bonds of the chain in the same way as in the antiferromagnetic Ising model. A defect (with symbol "1") occurs, if two neighbouring spins are aligned parallel, and no defect is present ("0"), if the spins point in opposite directions. Since a defect is defined on a bond, the defect dynamics for a spin flip $\alpha_i \to -\alpha_i$ is determined by the change of the triplet $(\alpha_{i-1}, \alpha_i, \alpha_{i+1}) \to (\alpha_{i-1}, -\alpha_i, \alpha_{i+1})$.[4] Consequently, spin flips of type (a) can give rise to two kinds of defect behaviour, depending on the value of the spin α_{i-1}:

1. Annihilation of two defects, e.g.,

$$\begin{aligned} \text{spin chain:} \quad & \ldots, +1, +1, +1, \ldots \to \ldots, +1, -1, +1, \ldots \\ \text{defects:} \quad & \ldots, 1, \quad 1, \ldots \quad \to \quad \ldots, 0, \quad 0, \ldots \end{aligned} \tag{11}$$

2. One defect moves to the left, e.g.,

$$\begin{aligned} \text{spin chain:} \quad & \ldots, -1, +1, +1, \ldots \to \ldots, -1, -1, +1, \ldots \\ \text{defects:} \quad & \ldots, 0, \quad 1, \ldots \quad \to \quad \ldots, 1, \quad 0, \ldots \end{aligned} \tag{12}$$

Both processes 1 or 2 occur with probability w_a per time step, if a triplet $(\alpha_{i-1}, \alpha_i, \alpha_{i+1})$ of the appropriate form is found in the spin chain $\boldsymbol{\alpha}$.

For the determination of attractors in the present parameter region we consider an orbit $\{\mathbf{x}^t\}$ of the CML that performs successive transitions of type (a). Each transition changes the defects of the corresponding spin chain $\boldsymbol{\alpha}$. Since only processes 1 and 2 are possible, defects can move to the left and annihilate in pairs. Consequently, the number of defects decreases monotonically.

[4] In order to have a simple translation of spin flips in the language of processes for defects, we assume that two neighbouring spins do not flip at the same time. As mentioned before, this is justified for $\epsilon, |\delta| \ll 1$, since in this case the average distance between lattice sites at which spins flip at the same time is rather large.

If the lattice size N is even, any spin chain contains an even number of defects. Therefore, in the final state all defects have annihilated each other and no further transitions of type (a) are possible. Hence, there are two attractors of the CML, the cubes $I_{(+1,-1,+1,-1,\ldots,-1,+1,-1)}$ and $I_{(-1,+1,-1,+1,\ldots,+1,-1,+1)}$.

For N odd the number of defects in a spin chain $\boldsymbol{\alpha}$ is odd. Consequently, at the end of the transient dynamics one defect remains. Since this defect can change its location via process 2 (cf. Eq. (12)), the attractor is the union of all $2N$ cubes $I_{\boldsymbol{\alpha}}$ for which $\boldsymbol{\alpha}$ contains a single "$+1+1$" or "$-1-1$" sequence.

In both cases the attractors occupy only a small portion of phase space for $N \gg 1$. Long transients occur in region 2, if one starts from random initial conditions.

In the coarse grained perspective the attractors correspond to antiferromagnetic ground states at zero temperature for the nearest neighbour Ising model. Of course, one would get these ground states also as stationary distributions of the master equation (8), if $w_a > 0$ and $w_b = 0$. Generally, stationary distributions of the master equation for the spin dynamics correspond to attractors of the underlying CML.

Region 3 ($\delta < -4\epsilon/3$). In this region transitions/spin flips of type (b) are possible, too. Depending on the left neighbour of the transition index, a type (b) spin flip can induce the following defect movements:

3. One defect moves to the right, e.g.,

$$\begin{aligned} \text{spin chain:} \quad & \ldots,-1,\ -1,\ +1,\ldots \rightarrow \ldots,-1,\ +1,\ +1,\ldots \\ \text{defects:} \quad & \ldots,\ 1,\quad 0,\ldots \quad \rightarrow \quad \ldots,\ 0,\quad 1,\ldots \end{aligned} \tag{13}$$

4. Two adjacent defects are generated simultaneously, e.g.,

$$\begin{aligned} \text{spin chain:} \quad & \ldots,+1,\ -1,\ +1,\ldots \rightarrow \ldots,\ +1,\ +1,\ +1,\ldots \\ \text{defects:} \quad & \ldots,\ 0,\quad 0,\ldots \quad \rightarrow \quad \ldots,\ 1,\quad 1,\ldots \end{aligned} \tag{14}$$

These two processes take place with a probability w_b per time step. Together with processes 1 and 2 in Eqs. (11) and (12), we have four different defect actions possible in region 3. Note that in general there is a bias in the defect diffusion, since for $w_a \neq w_b$ process 2 (Eq. (12)) and 3 (Eq. (13)) occur with different probability.

The ergodic behaviour of the CML in region 3 is simple, if one looks at attractors. Any index component α_i can change in the next cube change $I_{\boldsymbol{\alpha}} \rightarrow I_{\boldsymbol{\beta}}$ of an orbit. Therefore, there is a single attractor that encompasses all cubes $I_{\boldsymbol{\alpha}}$.

In the coarse grained perspective one asks for the stationary distribution $\mathbf{p}^{\text{stat}}$ of the master equation (8) that corresponds to this attractor. The stationary distribution fulfills the condition

$$\sum_{\boldsymbol{\beta} \neq \boldsymbol{\alpha}} [w(\boldsymbol{\alpha} \mid \boldsymbol{\beta}) \cdot p_{\boldsymbol{\beta}}^{\text{stat}} - w(\boldsymbol{\beta} \mid \boldsymbol{\alpha}) \cdot p_{\boldsymbol{\alpha}}^{\text{stat}}] = 0. \tag{15}$$

Here the transition probabilities $w(\boldsymbol{\beta} \mid \boldsymbol{\alpha})$ are given in Eq. (9). In Appendix C it is shown that this condition can be solved with

$$p_{\boldsymbol{\alpha}}^{\text{stat}} = c' \left(\frac{w_b}{w_a}\right)^{\sum_{i=1}^{N} \alpha_i \alpha_{i+1}/4} = \frac{1}{Z} \exp\left(\beta J \sum_{i=1}^{N} \alpha_i \alpha_{i+1}\right). \tag{16}$$

Therefore, as in region 2 the stationary distribution of the master equation corresponds to the canonical distribution of a nearest neighbour Ising model. However, in region 3 the temperature $T = 1/\beta$ of the canonical distribution is nonzero, as it is given by

$$\beta J = \frac{1}{4} \ln\left(\frac{w_b}{w_a}\right). \tag{17}$$

Taking a spin coupling J with modulus one, ferromagnetic coupling ($J = +1$) is obtained for $(w_b/w_a) > 1$, whereas in the opposite case $(w_b/w_a) < 1$ antiferromagnetic coupling ($J = -1$) follows. Both cases are realised in region 3 as shown by the gray shading in Fig. 2. In the antiferromagnetic part the temperature can take on all positive values, whereas in the ferromagnetic part only fairly high values are realised, since $(w_b/w_a) \lesssim 1.2$ in the perturbative regime. Spin coupling and diffusion bias are linked together: for ferromagnetic coupling defects diffuse preferably to the right, for antiferromagnetic coupling to the left. The cases with different coupling are separated by a line on which $w_a = w_b$ or $T = \infty$. This line can be calculated as $\delta = -2\epsilon$ (cf. Appendix A). There is also a large subset of region 3 on which $T = \infty$ holds (cf. Fig. 2), since according to Eq. (10) $w_a = w_b$ holds for $\delta < -4\epsilon$. One can also say that there is no spin interaction in this area of parameter space.

Next, we would like to address the question how much one can trust the presented results about the ergodic dynamics of the CML. Since we have only worked out the first order of perturbation theory, neglected higher order transitions might spoil the picture. However, numerical simulations indicate that the calculated attractors of region 2 are indeed reached for any initial condition of the CML and thereafter not left any more. So, higher order transitions do not seem to have any influence on the attractors in region 2. On a more general level, one can put forward the following

time scale argument concerning an attractor A that is determined in leading order perturbation theory. Higher order transitions through which an orbit could leave the set A occur on a rather large time scale in comparison to the relatively fast dominant transitions through which the orbit is pulled back to the set A again. Because of this intermittent dynamics the set A is at least the core region of a possibly bigger attractor, i.e., A carries most of the natural measure of that attractor. Likewise, there will be corrections to the Ising Hamiltonian that describes the stationary distribution $\mathbf{p}^{\text{stat}}$ of spin states in region 3 (cf. Eq. (16)). However, these correction terms are suppressed with a factor of the order $\mathcal{O}(\epsilon, \delta)$ in perturbation theory. The thermodynamic limit $N \to \infty$ poses no problem to the validity of the master equation (8) and its solution in (16). For, in the perturbation theory we have not neglected any changes of spin configuration that become more important for larger and larger N. Besides, the factors $(1-w^{(2)}(\alpha_i\ \alpha_{i+1} \to -\alpha_i\ \alpha_{i+1}))$ in Eq. (9) for the transition probabilities $w(\boldsymbol{\beta} \mid \boldsymbol{\alpha})$ ensure that the sum of all these transition probabilities stays finite for $N \to \infty$.

Finally, we compare the different ergodic behaviour in the 3 regions with the phases of the symmetrically coupled CML that has been analysed in ref. 8. In that case 4 regions with different ergodic behaviour have been found. On the level of attractors, the results for the two ways of coupling are rather similar. For $\delta \geqslant 0$ no transitions are possible in both cases. Furthermore, also the symmetrically coupled CML reaches an antiferromagnetic ground state in some region of parameter space, namely for $-4\epsilon/3 \leqslant \delta < -2\epsilon/3$. For $\delta < -4\epsilon/3$ the stationary distribution of the corresponding spin models can be characterised by an Ising Hamiltonian in both cases. However, there is an additional phase for symmetric coupling, region 2 of ref. 8 (for parameter values $-2\epsilon/3 < \delta < 0$), where many attractors coexist. Also there is no bias in defect diffusion for symmetric coupling of the CML, so that the dynamic properties of both CMLs are rather different. This will be taken up in the next section.

6. NON-EQUILIBRIUM BEHAVIOUR OF THE CML

We now take a closer look at the non-equilibrium behaviour of the CML $\mathbf{T}_{\epsilon,\delta}$ and its corresponding spin dynamics. The bias in the diffusion is the cause that the stationary distribution (16) does not obey detailed balance in region 3

$$w(\boldsymbol{\beta} \mid \boldsymbol{\alpha})\, p_{\alpha}^{\text{stat}} \neq w(\boldsymbol{\alpha} \mid \boldsymbol{\beta})\, p_{\beta}^{\text{stat}}.$$

This can be verified easily. We take the spin configuration $\boldsymbol{\beta}$ as equal to $\boldsymbol{\alpha}$, except that one defect is shifted to a neighbouring empty site. Then

$p_{\alpha}^{\text{stat}} = p_{\beta}^{\text{stat}}$ holds, but $w(\boldsymbol{\beta} \mid \boldsymbol{\alpha}) \neq w(\boldsymbol{\alpha} \mid \boldsymbol{\beta})$ because of the bias. Since detailed balance is violated, the one-way coupled CML describes a stationary non-equilibrium state (cf. refs. 3 and 2). It is remarkable that the distribution of spin configurations in this non-equilibrium state is nevertheless described by the Ising Hamiltonian. At $\delta_b = -4\epsilon/3$ the CML $\mathbf{T}_{\epsilon,\delta}$ undergoes a non-equilibrium phase transition, since as discussed in the last section we have antiferromagnetic order in region 2 and disorder in region 3 of parameter space. The phase transition occurs at temperature zero, in accordance with the one dimensional lattice and the short ranged spin interaction.

The violation of detailed balance in region 3 can be understood in yet another way. A net flux of defects goes around in the stationary non-equilibrium state. We define this flux as

$$f := \frac{1}{N}(\langle \#\text{ of defects that move to the left}\rangle - \langle \#\text{ of defects that move to the right}\rangle). \tag{18}$$

The expectation values are defined with respect to the stationary distribution of Eq. (16). If we consider defect configurations $\tilde{\boldsymbol{\alpha}}$ that correspond to spin chains $\boldsymbol{\alpha}$, we can rewrite the flux as

$$f = \frac{1}{N}(w_a\langle \#\text{ of ``01'' sequences in } \tilde{\boldsymbol{\alpha}}\rangle - w_b\langle \#\text{ of ``10'' sequences in } \tilde{\boldsymbol{\alpha}}\rangle). \tag{19}$$

This can be evaluated as

$$f = \frac{w_a - w_b}{4}(1 - c(2)). \tag{20}$$

Here the well–known (equal time) two spin correlation function of the one dimensional Ising model comes into play that is given as[11]

$$c(r) := \langle \alpha_i \alpha_{i+r}\rangle = (\tanh(\beta J))^{|r|} = \left(\frac{\sqrt{w_b/w_a} - 1}{\sqrt{w_b/w_a} + 1}\right)^{|r|}, \tag{21}$$

where we have used Eq. (17). Hence we get the final result for the flux of defects

$$f = \frac{w_a - w_b}{4}\left(1 - \left(\frac{\sqrt{w_b/w_a} - 1}{\sqrt{w_b/w_a} + 1}\right)^2\right). \tag{22}$$

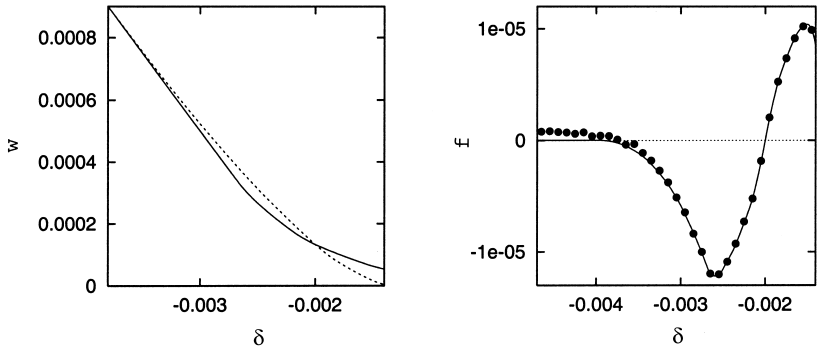

Fig. 3. Left: the two probabilities w_a (solid line) and w_b (broken line) that give rise to defect diffusion to the left and right, respectively, are shown as a function of the parameter δ (for fixed $\epsilon = 0.001$). Here w_a and w_b are calculated with the help of the theoretical formulas (A26) and (A21) that are derived in Appendix A. Both probabilities increase when δ decreases. For $\delta \approx -4\epsilon/3$ the probability w_b starts from zero, whereas w_a has already a finite value at that point. But w_b grows faster than w_a with decreasing δ, so w_b becomes greater than w_a for $\delta \lesssim -2\epsilon$. For even smaller values of δ the two probabilities approach equal values in accordance with Eq. (10). Right: the flux of defects is plotted against the deformation parameter δ where $\epsilon = 0.001$ stays again fixed. The points are obtained from simulations of the CML for these parameter values (the numerical errors are of the order of 1 to 3%). The solid line gives the theoretical prediction according to Eq. (22) where w_a and w_b are again determined from the expressions (A26) and (A21), respectively.

As shown in Appendix A, the probabilities w_a and w_b can be identified with the area of certain transition sets, the sets $U_{++,-+}$ and $U_{-+,++}$, respectively (cf. their definition in Eqs. (A25) and (A19)). On the left side of Fig. 3 the dependence of the two probabilities w_a and w_b with δ (for ϵ fixed) is shown where we have calculated the areas of the corresponding transition sets numerically. According to Eq. (22), the flux of defects is proportional to the difference $(w_a - w_b)$. Consequently, if $w_a > w_b$, defects diffuse preferably to the left; if $w_a < w_b$, defects move more often to the right. The direction of the current changes at the value of $\delta \approx -2\epsilon$ for which $w_a = w_b$ holds. Hence, the flux f can adopt positive and negative values as illustrated in the right part of Fig. 3. In this figure one can also see a very good agreement between the theoretical expression (20) and a numerical simulation of the CML in region 3.

Another quantity that is affected by the bias is the spatio-temporal two spin correlation function

$$\tilde{C}(r, \Delta t) := \langle \alpha_i(t)\, \alpha_{i+r}(t+\Delta t) \rangle. \tag{23}$$

Here the expectation value is performed again with respect to the stationary distribution of Eq. (16). Since this distribution is translationally invariant,

the quantity in Eq. (23) does not depend on the lattice index i. The calculation of the spatio-temporal correlation is carried out in Appendix B. The result for large lattices ($N \gg 1$) is

$$\tilde{C}(r, \Delta t) = \exp(-(w_a + w_b)\,\Delta t) \sum_{n=0}^{\infty} [c(1)]^{|n+r|} \frac{((w_b - w_a)\,\Delta t)^n}{n!} \tag{24}$$

where $c(1)$ denotes the equal time spin correlation for distance one in the Ising model (cf. Eq. (21)). Hence for $r \geqslant 0$

$$\tilde{C}(r, \Delta t) = [c(1)]^r \exp(-2\sqrt{w_a w_b}\,\Delta t). \tag{25}$$

For negative r and $w_a > w_b$ an asymptotic expansion for large times, i.e., $(w_a - w_b)\,\Delta t \gg 1$, gives (cf. Appendix B)

$$\tilde{C}(r, \Delta t) \simeq (-1)^r \sqrt{\frac{w_a}{w_b}}\, \exp(-2w_b \Delta t)\, \frac{\exp\left(-\dfrac{[(w_a - w_b)\,\Delta t + r]^2}{2(w_a - w_b)\,\Delta t}\right)}{\sqrt{2\pi(w_a - w_b)\,\Delta t}}. \tag{26}$$

According to this equation, in the antiferromagnetic regime the spatio-temporal correlation function develops a diffusive peak moving with velocity

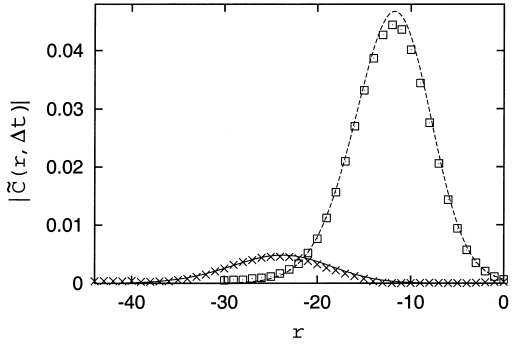

Fig. 4. Here we compare simulations of the modulus of the spatio-temporal correlation function $|\tilde{C}(r, \Delta t)|$ with theoretical predictions. We measured the spatio-temporal correlation function in CML simulations for two time differences $\Delta t = 50000$ (squares) and $\Delta t = 100000$ (crosses). The numerical errors of the simulation are approximately 1 to 3%. The theoretical prediction of the correlation function according to Eq. (24) is shown as a broken line. With increasing Δt the peak of the correlation function moves to the left and broadens. The parameters of the CML are taken as $\epsilon = 0.005$, $\delta = -0.007$. The corresponding transition rates for spin flips of type (a) and (b) are gained from a long time series of the CML and read $w_a \approx 0.000262$ and $w_b \approx 0.000020$. Hence, the coupling is strongly antiferromagnetic, so the correlation function $\tilde{C}(r, \Delta t)$ oscillates between positive and negative values.

$(w_a - w_b)$ to the left and spreading according to the diffusion constant $(w_a - w_b)$. This is illustrated in Fig. 4 where an excellent agreement between the CML simulations and the (exact) theoretical prediction of Eq. (24) is found.

From Eq. (25) and (26) one can infer

$$\tilde{C}(r, \Delta t) \neq \tilde{C}(-r, \Delta t), \qquad \Delta t > 0.$$

This asymmetry is caused by the diffusion bias and is not present for the equal time correlation functions ($\Delta t = 0$).

7. THE CASE OF STRONG COUPLING

As mentioned in Section 2 there is another range of coupling values ϵ where the unidirectional CML of Eq. (2) can be studied with a perturbative approach. In this case the coupling is very strong, i.e., $\epsilon = 1 - \eta$ and $\eta \ll 1$. Inserting this into Eq. (2) one obtains for the CML dynamics

$$x_i^{t+1} = \eta f_\delta(x_i^t) + (1-\eta)\, f_\delta(x_{i+1}^t), \qquad i = 1, 2, \ldots, N. \tag{27}$$

Accordingly, the value at lattice site i at time $t+1$ is mainly determined by its predecessor at the right neighbour site. We can treat the first term on the right of Eq. (27) as a perturbation, since $\eta \ll 1$. The analogy of the strong coupling regime to the one with $\epsilon \ll 1$ becomes even clearer, if one passes over to an inertial frame that moves in each time step one site to the left. For each time step $t \in \mathbb{N}$ this Galilei transformation can be written as

$$\tilde{x}_i^t = x_{i-t}^t, \qquad i = 1, 2, \ldots, N, \tag{28}$$

where periodic boundary are taken into account. The values $\tilde{x}_i^t$ constitute the CML in the moving frame. The dynamics in this frame is given by

$$\tilde{x}_i^{t+1} = (1-\eta)\, f_\delta(\tilde{x}_i^t) + \eta f_\delta(\tilde{x}_{i-1}^t), \qquad i = 1, 2, \ldots, N. \tag{29}$$

This is a CML with a small coupling strength η. The only difference of the last equation to Eq. (2) is that here the lattice site is coupled to its left neighbour.

To understand the dynamics of the strong coupling regime it is convenient to analyse Eq. (29) and then to transform back to the rest frame via the inverse of the Galilei transformation (28). In this manner one can infer two dominant transition types in the regime $\eta \ll 1$ that correspond to the discussed transition types (a) and (b) in the regime $\epsilon \ll 1$. The critical δ values of these transitions are $\delta_{\text{crit}} = 0$ and $\delta_{\text{crit}} = -4\eta/3$, respectively.

Therefore, for $\eta, |\delta| \ll 1$ one can again distinguish three parameter regions with different ergodic behaviour:

Region 1 ($\delta \geqslant 0$). There are no transitions in the moving inertial frame. Therefore each spin configuration $\boldsymbol{\alpha}^t$ is shifted one unit to the left in each time step:

$$\begin{aligned} \boldsymbol{\alpha}^t &: \quad \cdots + - + + - \cdots \\ \boldsymbol{\alpha}^{t+1} &: \quad \cdots + - + + - \cdots \end{aligned} \tag{30}$$

Region 2 ($-4\eta/3 < \delta < 0$). Here transitions/spin flips of the form

$$\begin{aligned} \boldsymbol{\alpha}^t &: \quad \cdots + + - \cdots \\ \boldsymbol{\alpha}^{t+1} &: \quad \cdots + + + \cdots \end{aligned} \tag{31}$$

and those related by symmetry are allowed. Therefore there is only one attractor (for N even) that is an antiferromagnetic ground state that moves with unit velocity to the left.

Region 3 ($\delta < -4\eta/3$). Here also the inverse transition to the one of Eq. (31) occurs. Therefore the attractor corresponds to an Ising chain at finite temperature that moves with unit velocity to the left.

That small and strong coupling are so closely related is peculiar to the unidirectional coupling. For a symmetrically coupled CML where two nearest neighbours interact with a lattice site this duality of weak and strong coupling no longer holds.

8. SUMMARY

In the present article we have analysed a spatially one dimensional coupled map lattice with an unidirectional local coupling. In order to obtain analytic results, we have confined ourselves to a perturbative regime in which the coupling strength is small and the single site map f_δ is taken in the vicinity of a symmetry breaking bifurcation. Via a coarse graining the CML could be mapped to a stochastic spin dynamics with an anisotropic local interaction. Because of a Markov behaviour in the perturbative regime, a master equation could be written down that describes the spin dynamics quantitatively.

In perturbation theory there are three regions in parameter space with different ergodic behaviour of the CML and different spin dynamics. These regions are separated by bifurcation lines of which the leading order could be calculated analytically by analysing a CML with only two sites. As in the CML with a symmetric coupling that has been studied in ref. 8, the

stationary distribution of the master equation can be identified with a canonical distribution of the nearest neighbour Ising model. The temperature and the sign of the spin coupling constant can be calculated from the microscopic parameters of the CML. Antiferromagnetic coupling is predominant in the perturbative regime. Also like in ref. 8, there exists a whole region where the spin dynamics runs into a totally ordered antiferromagnetic state at zero temperature. The CML also has a phase transition from antiferromagnetic order to disorder at zero temperature.

However, in contrast to the results in ref. 8 detailed balance is violated for the unidirectional CML, so that it describes a stationary non-equilibrium state. The non-equilibrium behaviour is caused by a bias in the diffusion of defects that gives rise to a macroscopic defect flux. These transport phenomena can also be detected in the spatio-temporal two spin correlation function.

Of course, our approach is not mathematically rigorous, but we have good indication that the results are valid at least in the perturbative regime. The comparison with numerical simulations shows that the leading order of perturbation theory is a good description for parameter values ϵ, $|\delta| \lesssim 5 \cdot 10^{-2}$.

As a project for the next future, we would like to go beyond perturbation theory in CMLs with local coupling. Then it will no longer be the case that a local coupling in the CML gives rise to local coupling in the corresponding spin model. We expect that for large coupling we have long-ranged interactions between spins. Besides, the Markov property will no longer hold in this case. Therefore, a non-perturbative approach poses quite a challenge even for CMLs in one spatial dimension.

APPENDIX A. THE CML FOR $N=2$

As discussed in Section 3, for the analysis of dominant transitions $\alpha_i\alpha_{i+1} \to -\alpha_i\alpha_{i+1}$ one can reduce the CML dynamics to the dynamics of the transition coordinate x_i^t and its neighbour x_{i+1}^t. Therefore, a CML with two sites ($N=2$) suffices for the understanding of the transitions of type (a) and (b) that are listed in Eqs. (4) and (5). In this appendix we analyse the corresponding transitions $I_{\alpha_1,\alpha_2} \to I_{-\alpha_1,\alpha_2}$ of the CML with $N=2$ rather extensively. The geometric method that we will employ can be easily visualised in the two dimensional phase space. Because of the unidirectional coupling in the CML $\mathbf{T}_{\epsilon,\delta}$ we couple the coordinate x_1^t to the coordinate x_2^t, but not vice versa. Hence the CML dynamics for $N=2$ can be written as

$$x_1^{t+1} = (1-\epsilon)\, f_\delta(x_1^t) + \epsilon f_\delta(x_2^t), \qquad x_2^{t+1} = f_\delta(x_2^t). \tag{A1}$$

In order that a phase space point can be mapped from a square I_α to a square I_β ($\beta_1 = -\alpha_1$, $\beta_2 = \alpha_2$), the image of the former square has to intersect the latter. Therefore, the overlap set

$$O_{\alpha,\beta} := \mathbf{T}_{\epsilon,\delta}(I_\alpha) \cap I_\beta \tag{A2}$$

has to be non-empty. However, in order that a transition $I_\alpha \to I_\beta$ becomes possible, the overlap set $O_{\alpha,\beta}$ has to be reachable by an orbit that starts in the inner part[5] of the square I_α. To check this condition we investigate the pre-images of the overlap set $O_{\alpha,\beta}$ that are contained in I_α. The pre-images of generation k are defined in the following recursive way

$$\begin{aligned} &\mathbf{T}_{\epsilon,\delta}^{-1}(O_{\alpha,\beta}) := \{\mathbf{x} \in I_\alpha \mid \mathbf{T}_{\epsilon,\delta}(\mathbf{x}) \in O_{\alpha,\beta}\}, \\ &\mathbf{T}_{\epsilon,\delta}^{-k}(O_{\alpha,\beta}) := \{\mathbf{x} \in I_\alpha \mid \mathbf{T}_{\epsilon,\delta}(\mathbf{x}) \in \mathbf{T}_{\epsilon,\delta}^{-(k-1)}(O_{\alpha,\beta})\}\,, \qquad k = 2, 3, \ldots. \end{aligned} \tag{A3}$$

We start with the detailed analysis of the transition $I_{-+} \to I_{++}$ that is related to transition type (b) (cf. Eq. (A3)). Here and in the following we write "+" instead of "+1" and "−" instead of "−1".

A.1. THE TRANSITION $I_{-+} \to I_{++}$

The overlap set $O_{-+,++}$ (cf. its definition in Eq. (A2)) is non-empty for general δ and displayed in Fig. 5 for $\delta = -\epsilon$. It can be shown that most points $\mathbf{x} \in O_{-+,++}$ wander towards the center of the square I_{++} under further iteration, exceptional points having a negligible area of size $O(\epsilon^2, \delta^2, \epsilon\delta)$. Hence, if the overlap set $O_{-+,++}$ can be reached by orbits $\{\mathbf{x}^t, t = 0, 1, 2, \ldots\}$ with starting point $\mathbf{x}^0$ in the inner part of I_{-+}, then a transition $I_{-+} \to I_{++}$ is possible. This condition will also determine the critical value $\delta_{\text{crit}}(\epsilon)$ of this transition. Therefore, for given parameters ϵ, δ we trace back the points of the overlap set and construct pre-image sets $\mathbf{T}_{\epsilon,\delta}^{-k}(O_{-+,++})$ in I_{-+} (cf. definition in Eq. (A3)).

Instead of the CML dynamics in Eq. (A1), we can use the following simplified map for the calculation of pre-images in the perturbative regime

$$\begin{aligned} [\tilde{\mathbf{T}}_{\epsilon,\delta}(\mathbf{x})]_1 &= f_\delta(x_1) + \epsilon f_{\delta=0}(x_2), \\ [\tilde{\mathbf{T}}_{\epsilon,\delta}(\mathbf{x})]_2 &= f_{\delta=0}(x_2). \end{aligned} \tag{A4}$$

[5] For our perturbative treatment we define the inner part of I_α as the set of all $\mathbf{x} \in I_\alpha$ which have at least a small fixed positive distance d from the boundary of this square. The quantity d should not depend on the expansion parameters ϵ and δ.

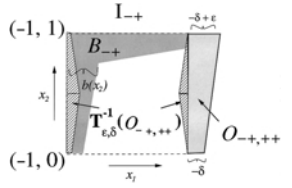

Fig. 5. Overlap set $O_{-+,++}$ and its pre-image set $\mathbf{T}^{-1}_{\epsilon,\delta}(O_{-+,++})$ are shown for $\delta = -\epsilon$. The forbidden area $B_{-+} \subset I_{-+}$ contains the pre-images of $O_{-+,++}$ on the left side.

In Fig. 5 the first generation pre-images of the overlap set are displayed (for $\delta = -\epsilon$): because of the tent shape of the single site map $f_\delta(x)$ the pre-images are located either near the right ($x_1 = \mathcal{O}(\epsilon, \delta)$) or the left edge ($x_1 = -1 + \mathcal{O}(\epsilon, \delta)$) of the square I_{-+}. At this stage the forbidden area comes into play. The forbidden area B_{-+} is the set of points in I_{-+} that do not have pre-images with respect to the map $\tilde{\mathbf{T}}_{\epsilon,\delta}$. This set is non-empty, since the map $\tilde{\mathbf{T}}_{\epsilon,\delta}$ is not surjective. The width of the set B_{-+} near the left edge of I_{-+} is given as (cf. Fig. 5)

$$b(x_2) = \epsilon + \epsilon x_2\,, \qquad x_2 \in [0, 1]. \tag{A5}$$

Points of $\tilde{\mathbf{T}}^{-1}_{\epsilon,\delta}(O_{-+,++})$ on the left side of I_{-+} are contained in the forbidden area for this choice of parameters (cf. Fig. 5). Then these points have no pre-images themselves.

Let us define the right and left components of the pre-image sets $\mathbf{x} \in \tilde{\mathbf{T}}^{-k}_{\epsilon,\delta}(O_{-+,++})$ as follows

$$\begin{aligned} G^{(k)} &:= \{\mathbf{x} \in \tilde{\mathbf{T}}^{-k}_{\epsilon,\delta}(O_{-+,++}) \,|\, x_1 = \mathcal{O}(\epsilon, \delta)\}, \\ H^{(k)} &:= \{\mathbf{x} \in \tilde{\mathbf{T}}^{-k}_{\epsilon,\delta}(O_{-+,++}) \,|\, x_1 = -1 + \mathcal{O}(\epsilon, \delta)\}. \end{aligned} \tag{A6}$$

We first concentrate on the sets $\{G^{(k)}\}$. Figure 6 (left side) reveals a beautiful structure of these sets. The following properties of the generations $G^{(k)}$ that are inherent in Fig. 6 are easily obtained:

- The first generation $G^{(1)}$ consists of two triangles with vertices $\{(0, 0), (0, 1/2), (-\epsilon/2, 1/2)\}$ and $\{(0, 1), (0, 1/2), (-\epsilon/2, 1/2)\}$, respectively.

- A generation $G^{(k)}$ encompasses 2^k triangles, each of them having the same area. The area of each triangle shrinks by a factor 4, if one passes from $G^{(k-1)}$ to $G^{(k)}$.

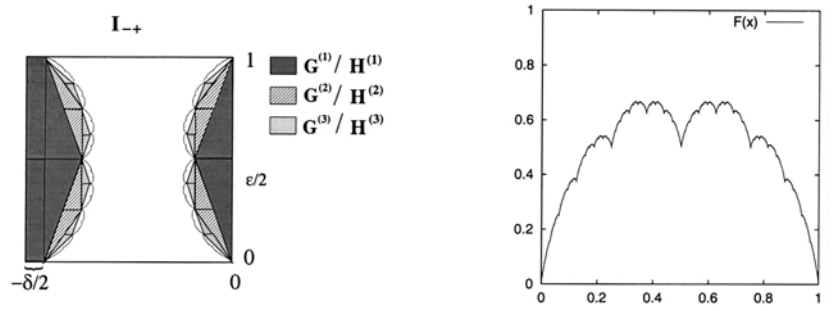

Fig. 6. Left: The first three generations $G^{(k)}$ and $H^{(k)}$ near the right and left edge of I_{-+}, respectively. The envelopes R^{∞} and S^{∞} of all pre-image sets $G^{(k)}$ and $H^{(k)}$, respectively, are related to the Takagi function. Right: Takagi function $F(x)$.

- Two neighbouring triangles of the same generation share a corner or a side with length of order ϵ.
- The union of the first k generations

$$\Sigma_G^{(k)} := \bigcup_{n=1}^{k} G^{(n)} \tag{A7}$$

is a simply connected set.

To determine the boundary of $\Sigma_G^{(k)}$ we consider its height function

$$R^{(k)}(x_2) := \inf\{x_1 \mid (x_1, x_2) \in \Sigma_G^{(k)}\}. \tag{A8}$$

Since $R^{(k+1)}$ is mapped on $R^{(k)}$ by the simplified map $\tilde{\mathbf{T}}_{\epsilon,\delta}$ (Eq. (A4)), we get the representation

$$R^{(k)}(x_2) = -\epsilon \sum_{i=1}^{k} \frac{f_{\delta=0}^{i}(x_2)}{2^i}, \qquad x_2 \in [0, 1]. \tag{A9}$$

For k odd these curves admit $2^{(k-1)/2}$ absolute maxima at

$$x_{\min} \in \left\{ \frac{1}{2}\left(1 + \sum_{j=1}^{(k-1)/2} \frac{i_j}{4^j}\right) \middle| \, i_j \in \{-1, +1\},\ j = 1, 2, \ldots, (k-1)/2 \right\} \tag{A10}$$

of equal height

$$R^{(k)}(x_{\min}) = -\frac{\epsilon}{2} \sum_{i=0}^{(k-1)/2} \frac{1}{4^i}. \tag{A11}$$

In the limit $k \to \infty$ the set Σ_G^∞ has a fractal boundary. The boundary function is given by

$$R^\infty(x_2) = \lim_{k\to\infty} R^{(k)}(x_2) = -\epsilon \sum_{i=1}^{\infty} \frac{f^i_{\delta=0}(x_2)}{2^i} = -\epsilon F(x_2). \tag{A12}$$

Here $F(x)$ is the famous Takagi function, a prominent example of a continuous but nowhere differentiable function. This function is displayed on the right side of Fig. 6 and shows a high degree of self-similarity. It is amusing to note that the Takagi function $F(x)$ that has already been introduced in 1903 has shown up in various recent studies of dynamical systems. [13, 14] The height of the set Σ_G^∞ follows easily from Eq. (A11)

$$h(\Sigma_G^\infty) := \sup\{|x_1| \,|\, \mathbf{x} \in \Sigma_G^\infty\} = \frac{2\epsilon}{3}. \tag{A13}$$

The extension of the set Σ_G^∞ is approximately independent of the parameter δ and does not contain any points that belong to the inner part of I_{-+}. Hence, we have to look for the sets $\{H^{(k)}\}$ near the left edge of I_{-+} in order to determine the critical value for δ. The location of the pre-image sets $\{H^{(k)}\}$ can be determined, if one knows the sets $\{G^{(k)}\}$, since both sets $H^{(k)}$ and $G^{(k)}$ are pre-images of the set $G^{(k-1)}$ (if $\delta > \delta_{\text{crit}}(\epsilon)$). Therefore, the set $H^{(k)}$ ($k \geqslant 2$) can be obtained geometrically through a reflection of the set $G^{(k)}$ at the line $x_1 = -1/2$ and an additional offset $-\delta/2$ (cf. left side of Fig. 6). This carries over to the union set $\Sigma_H^\infty := \bigcup_{k=1}^\infty H^{(k)}$. In analogy to equation (A9) the right boundary of the set Σ_H^∞ can be expressed with the Takagi function as

$$S^\infty(x_2) := \sup\{x_1 \,|\, (x_1, x_2) \in \Sigma_G^\infty\} = -1 - \frac{\delta}{2} + \epsilon F(x_2)\,, \qquad x_2 \in [0, 1]. \tag{A14}$$

Hence, the thickness of Σ_H^∞ is given by

$$h(\Sigma_H^\infty) := \sup\{1 + x_1 \,|\, \mathbf{x} \in \Sigma_H^\infty\} = -\frac{\delta}{2} + \frac{2\epsilon}{3}. \tag{A15}$$

If all left components $H^{(k)}$ are contained in the forbidden area, i.e.,

$$\Sigma_H^\infty \subset B_{-+} \tag{A16}$$

holds, no further pre-images of the overlap set $O_{-+,++}$ appear, and the union $\Sigma_G^\infty \cup \Sigma_H^\infty$ encompasses all pre-images. Then the transition $I_{-+} \to I_{++}$ is not

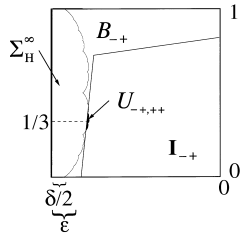

Fig. 7. Non-empty transition set $U_{-+,++} := \Sigma_H^\infty \setminus B_{-+}$ for δ slightly smaller than $\delta_{\text{crit}}(\epsilon)$. The set Σ_H^∞ is no longer contained in the forbidden area B_{-+} for these δ values.

possible, because all pre-images of the overlap set are located near the edge of I_{-+} and contain no point of the inner part of I_{-+}. Therefore, condition (A16) gives the clue for the determination of $\delta_{\text{crit}}(\epsilon)$. At the critical value $\delta_{\text{crit}}(\epsilon)$ one peak of the boundary Σ_H^∞ with maximal height $h(\Sigma_H^\infty)$ collides with the right border of the forbidden area B_{-+} (cf. Fig. 7). Since the boundary of the forbidden area has according to Eq. (A5) a finite slope, the peak with the smallest x_2 coordinate crosses the right boundary of B_{-+} at first.[6] According to Eq. (A10) this peak is located at $x_2 = 1/3$. Then Eqs. (A15) and (A5) yield

$$\frac{2}{3}\epsilon - \frac{\delta_{\text{crit}}(\epsilon)}{2} = h(\Sigma_H^\infty) = b(x_2 = 1/3) = \frac{4}{3}\epsilon, \tag{A17}$$

and consequently we arrive at the critical value

$$\delta_{\text{crit}}(\epsilon) = -\tfrac{4}{3}\epsilon. \tag{A18}$$

Therewith we have also determined the leading order of the critical value δ_b for type (b) transitions in the CML $\mathbf{T}_{\epsilon,\delta}$ (cf. Eq. (6)).

For the transition $I_{-+} \to I_{++}$ we can define the transition set $U_{-+,++}$ as

$$U_{-+,++} := \Sigma_H^\infty \setminus B_{-+}. \tag{A19}$$

This set becomes non-empty for $\delta < \delta_{\text{crit}}(\epsilon)$ (cf. Fig. 7). An orbit $\mathbf{x}^t$ performs a transition $I_{-+} \to I_{++}$, if it enters the set $U_{-+,++}$ at time t_0. For the transition coordinate $x_1^{t_0} \approx -1$ and $x_1^{t_0+1} = \mathcal{O}(\epsilon, \delta)$ holds. The set $U_{-+,++}$

[6] This can be shown rigorously with the inequality

$$\sup\{x_1 \mid (x_1, x_2) \in \Sigma_H^\infty\} \leqslant \sup\{x_1 \mid (x_1, 1/3) \in \Sigma_H^\infty\} + \epsilon(x_2 - \tfrac{1}{3}).$$

has a pre-image set $\mathbf{T}_{\epsilon,\delta}^{-1}(U_{-+,++})$ to which points $\mathbf{x}$ in the inner part of I_{-+} belong ($x_1 \approx -\frac{1}{2}$). Hence, the overlap set $O_{-+,++}$ can be reached by orbits with starting point in the inner part of I_{-+}, so the transition $I_{-+} \to I_{++}$ is possible for $\delta < \delta_{\text{crit}}(\epsilon)$.

Next, we would like to calculate the transition rate, i.e., the probability per time step for the transition $I_{-+} \to I_{++}$ that appears in the master equation (8) for the CML. Before the transition occurs, an orbit stays a rather long time in the square I_{-+}. Since $\mathbf{T}_{\epsilon,\delta}$ is a perturbed tent map, the elements of the orbit are distributed quite homogeneously in this square. If the orbit reaches the set $\mathbf{T}_{\epsilon,\delta}^{-1}(U_{-+,++})$, a transition follows. Therefore, in a statistical perspective the leading order of the transition probability is given as

$$w^{(2)}(-+ \to ++) = \frac{\text{Area}(\mathbf{T}_{\epsilon,\delta}^{-1}(U_{-+,++}))}{\text{Area}(I_{-+})} = \text{Area}(U_{-+,++}). \tag{A20}$$

We have thus linked the transition probability with the area of the transition set $U_{-+,++}$ (cf. Fig. 7). The area of the set $U_{-+,++}$ can be expressed with the help of Eqs. (A14) and (A5), and we get for the transition probability

$$w^{(2)}(-+ \to ++) = \int_0^1 dx_2 \max\left\{0, -\frac{\delta}{2} + \epsilon F(x_2) - \epsilon(1+x_2)\right\}. \tag{A21}$$

One can infer from this expression that the transition probability increases monotonically as δ becomes smaller. Since the Takagi function $F(x)$ has a complicated graph (cf. Fig. 6), it is very tedious to evaluate Eq. (A21) for general ϵ, δ. On the left side of Fig. 3 a numerical evaluation of expression (A21) is shown for varying δ and ϵ fixed (the curve for the probability w_b). However, for $\delta \leqslant -4\epsilon$ it can be found

$$w^{(2)}(-+ \to ++) = -\frac{\delta}{2} - \epsilon. \tag{A22}$$

In addition, using the (partial) self-similarity of the Takagi function one can compute the transition probability for selected δ values that accumulate at the critical value $\delta_{\text{crit}}(\epsilon) = \delta_b = -4\epsilon/3$

$$w^{(2)}(-+ \to ++) = \frac{\epsilon}{60 \cdot 8^{k-1}} \qquad \text{for} \quad \delta = \delta_b - \frac{2\epsilon}{3 \cdot 4^k}, \quad k = 0, 1, 2, \ldots \tag{A23}$$

Hence we infer the asymptotic property

$$w^{(2)}(-+ \to ++) \sim \epsilon \left(\frac{\delta_b - \delta}{\epsilon} \right)^{3/2}, \qquad (\delta < \delta_b). \tag{A24}$$

Equation (A24) together with Eq. (17) indicates that scaling at the phase transition and the numerical values of the critical exponents may strongly depend on whether such a behaviour is evaluated in dependence on the actual map parameters or in terms of the appropriate temperature of the corresponding spin model.

A.2. THE TRANSITION $I_{++} \to I_{-+}$

The transition $I_{++} \to I_{-+}$ corresponds to transition type (a) of Eq. (5). The study of this transition is quite analogous to that of the transition $I_{-+} \to I_{++}$, so that we will be rather brief in the following. The overlap set $O_{++,-+}$ is non-empty for $\delta < 0$. On the left of Fig. 8 this overlap set and its pre-images are shown for $\delta \approx -\epsilon$. The pre-image set $\mathbf{T}^{-1}_{\epsilon,\delta}(O_{++,-+})$ is located near the right edge of I_{++} ($x_1 \approx 1$). There is also a forbidden area B_{++} in the square I_{++}. However, it is important to notice that not the whole pre-image set $\mathbf{T}^{-1}_{\epsilon,\delta}(O_{++,-+})$ is contained in the forbidden area (cf. left side of Fig. 8). This holds for arbitrary $\delta < 0$, and thus the pre-image set of second generation $\mathbf{T}^{-2}_{\epsilon,\delta}(O_{++,-+})$ is non-empty (cf. Fig. 8) and

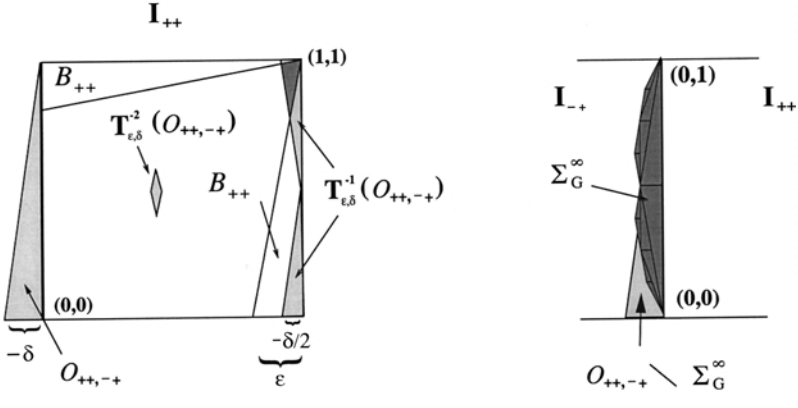

Fig. 8. Left: Overlap set $O_{++,-+}$ and pre-image sets of first and second generation are shown. Note that the dark shaded subset of $\mathbf{T}^{-1}_{\epsilon,\delta}(O_{++,-+})$ is located outside the forbidden area B_{++}. Right: The overlap set $O_{++,-+}$ intersects the set Σ^{∞}_{G} (approximated here by three pre-image generations).

is located in the inner part of I_{++} ($x_1 \approx 1/2$). Since the union of pre-image sets $\mathbf{T}_{\epsilon,\delta}^{-k}(O_{++,-+})$ with $k \geqslant 2$ has a substantial volume in the inner part of I_{++}, the transition $I_{++} \to I_{-+}$ is possible for $\delta < 0$. Hence we find $\delta_{\text{crit}}(\epsilon) = 0$ as the critical value for this transition and thus have derived $\delta_a = 0$ in Eq. (6).

Concerning the calculation of the transition rate $w^{(2)}(++ \to -+)$ note that not all points of the overlap set $O_{++,-+}$ reach the inner part of I_{-+} upon further iteration. For, the set Σ_G^∞, that has been introduced in the last subsection (cf. Eq. (A7)), intersects the overlap set $O_{++,-+}$ (cf. right part of Fig. 8). Points of Σ_G^∞ wander back into the square I_{++} under further iteration. Besides, one has to take into account that a major part of the pre-image set (of first generation) $\mathbf{T}_{\epsilon,\delta}^{-1}(O_{++,-+})$ is contained in the forbidden area B_{++}. Hence, only points of the transition set

$$U_{++,-+} := \{\mathbf{x} \in \mathbf{T}_{\epsilon,\delta}^{-1}(O_{++,-+}) \setminus B_{++} \mid \mathbf{T}_{\epsilon,\delta}(\mathbf{x}) \in O_{++,-+} \setminus \Sigma_G^\infty\} \tag{A25}$$

perform a transition to the inner part of I_{-+}. In a statistical perspective we arrive at a transition probability

$$\begin{aligned} w^{(2)}(++ \to -+) &= \text{Area}(U_{++,-+}) \\ &= \frac{1}{4}\left(\int_0^1 dx_2 (\max\{0, -\delta - 2\epsilon x_2 + R^\infty(x_2)\}\right. \\ &\quad \left. + \max\{0, -\delta - 2\epsilon + R^\infty(x_2)\})\right), \end{aligned} \tag{A26}$$

where $R^\infty(x_2)$ is the boundary function of Σ_G^∞ and is given in Eq. (A12). We have two summands under the integral of equation (A26) because of the two components of the set $\mathbf{T}_{\epsilon,\delta}^{-1}(O_{++,-+})$ (cf. left side of Fig. 8). A numerical evaluation of Eq. (A26) is shown on the left side of Fig. 3 (the curve of the probability w_a).

Finally, we could evaluate equation (A26) for the transition rate $w(++ \to -+)$ analytically for the following parameter values

$$\begin{aligned} w^{(2)}(-+ \to ++) &= -\frac{\delta}{2} - \epsilon, \qquad \delta < -\frac{8}{3}\epsilon, \\ w^{(2)}(-+ \to ++) &= \frac{2\epsilon}{15}, \qquad\qquad \delta = -2\epsilon. \end{aligned} \tag{A27}$$

APPENDIX B. THE SPATIO-TEMPORAL CORRELATION FUNCTION

In this appendix we will calculate the spatio-temporal two spin correlation function of the CML induced spin dynamics in region 3, i.e., we derive Eq. (24).

First, we pass over from a discrete time variable ($t \in \mathbb{N}$) to a continuous one ($\tau \in \mathbb{R}^+$) by introducing a scaled time $\tau = \epsilon t$. The time variable τ becomes a continuous variable in the limit $\epsilon \to 0$, keeping the ratio δ/ϵ fixed. The introduction of a continuous time is a good approximation in the perturbative regime ($\epsilon, |\delta| \ll 1$) and simplifies calculations. In this approach the master equation (8) for the spin dynamics becomes a differential equation

$$\frac{dp_{\alpha}(\tau)}{d\tau} = \sum_{\beta \neq \alpha} [r(\boldsymbol{\alpha} \mid \boldsymbol{\beta}) \cdot p_{\beta}(\tau) - r(\boldsymbol{\beta} \mid \boldsymbol{\alpha}) \cdot p_{\alpha}(\tau)]. \tag{B1}$$

For fixed system size N, in the limit $\epsilon, |\delta| \to 0$ those transitions $\boldsymbol{\alpha} \to \boldsymbol{\beta}$ dominate where only one spin flips, i.e., $\beta_i = -\alpha_i$, $\beta_j = \alpha_j \ \forall j \neq i$. For, according to Eq. (9) all transitions $\boldsymbol{\alpha} \to \boldsymbol{\beta}$ with more than one spin flip are suppressed by a factor $\mathcal{O}(\epsilon, \delta)$ in perturbation theory, because each spin flip probability $w^{(2)}(\alpha_i \alpha_{i+1} \to -\alpha_i \alpha_{i+1})$ has a magnitude of the order $\mathcal{O}(\epsilon, \delta)$. Hence, in the differential equation (B1) we have only to sum over spin states $\boldsymbol{\beta}$ which differ from $\boldsymbol{\alpha}$ in one spin. The transition rates $r(\boldsymbol{\beta} \mid \boldsymbol{\alpha})$ in Eq. (B1) are related to the transition probabilities $w(\boldsymbol{\beta} \mid \boldsymbol{\alpha})$ in Eq. (9) as follows

$$\begin{aligned} r(\boldsymbol{\beta} \mid \boldsymbol{\alpha}) &= \lim_{\epsilon \to 0} \frac{w(\boldsymbol{\beta} \mid \boldsymbol{\alpha})}{\epsilon} = \lim_{\epsilon \to 0} \frac{w^{(2)}(\alpha_i \alpha_{i+1} \to -\alpha_i \alpha_{i+1})}{\epsilon} \delta_{-\alpha_i, \beta_i} \prod_{j(\neq i)} \delta_{\alpha_j, \beta_j} \\ &=: \frac{R}{2} (1 - \gamma\, \alpha_i \alpha_{i+1})\, \delta_{-\alpha_i, \beta_i} \prod_{j(\neq i)} \delta_{\alpha_j, \beta_j}. \end{aligned} \tag{B2}$$

The parameters R and γ related to the transition probabilities w_a and w_b for the two possible spin flip types $\alpha_i \alpha_{i+1} \to -\alpha_i \alpha_{i+1}$ as follows

$$R = \lim_{\epsilon \to 0} \frac{w_a + w_b}{\epsilon}, \qquad \gamma = \lim_{\epsilon \to 0} \frac{w_b - w_a}{w_a + w_b}. \tag{B3}$$

Note that according to Eq. (B2) only the right nearest neighbour and not the left one influences the transition rates.

The spatio-temporal two spin correlation function of Eq. (23) can be written as

$$\tilde{C}(r, \Delta\tau) = \sum_{\{\alpha, \alpha'\}} p_{\alpha}^{\text{stat}} \alpha_i \, p(\boldsymbol{\alpha}\,; \tau \mid \boldsymbol{\alpha}'; \tau + \Delta\tau)\, \alpha'_{i+r}. \tag{B4}$$

Here $p(\boldsymbol{\alpha}; \tau \mid \boldsymbol{\alpha}'; \tau + \Delta\tau)$ denotes the conditional probability for a configuration $\boldsymbol{\alpha}'$ at time $\tau + \Delta\tau$, if at time τ the configuration $\boldsymbol{\alpha}$ is present. Since the conditional probability also obeys the master equation (B1), the following system of differential equations follows from the master equation and the rates (B2)

$$\frac{\partial}{\partial \Delta\tau} \tilde{C}(r, \Delta\tau) = -R(\tilde{C}(r, \Delta\tau) - \gamma \tilde{C}(r+1, \Delta\tau)). \tag{B5}$$

Introducing the spatial Fourier transform

$$\tilde{\Gamma}(q, \Delta\tau) := \sum_{r=-\infty}^{\infty} e^{iqr} \tilde{C}(r, \Delta\tau) \tag{B6}$$

the system decouples

$$\frac{\partial}{\partial \Delta\tau} \tilde{\Gamma}(q, \Delta\tau) = -R(1 - \gamma e^{-iq})\, \tilde{\Gamma}(q, \Delta\tau), \tag{B7}$$

where the initial condition is given by the Fourier transform of the equal time correlation function (21)

$$\tilde{\Gamma}(q, 0) = 1 + \frac{e^{iq} c(1)}{1 - e^{iq} c(1)} + \frac{e^{-iq} c(1)}{1 - e^{-iq} c(1)}. \tag{B8}$$

Integrating Eq. (B7), taking the inverse Fourier transform and finally expressing R and γ in terms of w_a and w_b according to Eq. (B3) and changing to original discrete time, we arrive at the integral representation of the correlation function for $N \gg 1$

$$\tilde{C}(r, \Delta t) = \frac{1}{2\pi} \exp(-(w_a + w_b)\, \Delta t) \int_0^{2\pi} \tilde{\Gamma}(q, 0) \exp(e^{-iq}(w_b - w_a)\, \Delta t - iqr)\, dq. \tag{B9}$$

The series representation (24) follows by using the Taylor series expansion

$$\exp(e^{-iq}(w_b - w_a)\, \Delta t) = \sum_{n=0}^{\infty} \frac{((w_b - w_a)\, \Delta t)^n}{n!} e^{-iqn}. \tag{B10}$$

In order to derive the asymptotic result (26) we use the Laplace method and expand the exponential under the integral in Eq. (B9) at $q = \pi$ to second order

$$\tilde{C}(r, \Delta t) \simeq \frac{1}{2\pi} \exp(-(w_a + w_b)\,\Delta t)\, e^{-i\pi r} \int_{-\infty}^{\infty} \tilde{\Gamma}(\pi, 0) \times \exp((w_a - w_b)\,\Delta t[1 - q^2/2] - iq((w_a - w_b) + r))\, dq. \tag{B11}$$

Evaluation of the resulting Gaussian integral yields Eq. (26). Since the exponent contains an imaginary part, the Laplace method cannot be applied in the strict sense. That feature modifies the Gaussian tails of our asymptotic result.

APPENDIX C. THE MASTER EQUATION FOR THE CML

In this appendix we will first give an argument for the form of the transition probability $w(\boldsymbol{\alpha} \mid \boldsymbol{\beta})$ in Eq. (9). Then we will show that the stationary distribution of Eq. (16) solves the master equation (8) with these transition probabilities.

To get an expression for $w(\boldsymbol{\alpha} \mid \boldsymbol{\beta})$ we will analyse the underlying dynamics of the CML $\mathbf{T}_{\epsilon,\delta}$ in perturbation theory. The transition probability $w(\boldsymbol{\alpha} \mid \boldsymbol{\beta})$ per time step for a change of spin configuration $\boldsymbol{\alpha} \to \boldsymbol{\beta}$ can be interpreted in the following geometric way

$$w(\boldsymbol{\beta} \mid \boldsymbol{\alpha}) = \frac{\mathrm{Vol}(S(\boldsymbol{\alpha} \to \boldsymbol{\beta}))}{\mathrm{Vol}(Q(\boldsymbol{\alpha}))}. \tag{C1}$$

The two involved subsets of phase space are defined as

$$Q(\boldsymbol{\alpha}) := \{\text{points } \mathbf{x}^t \text{ of phase space that can be reached by CML orbits, if the corresponding spin state is } \boldsymbol{\alpha}\}$$

$$S(\boldsymbol{\alpha} \to \boldsymbol{\beta}) := \{\text{points } \mathbf{x}^{t_0} \text{ of CML orbits that perform a change of spin configuration } \boldsymbol{\alpha} \to \boldsymbol{\beta} \text{ at time } t_0\}$$

In perturbation theory the volume of the set $Q(\boldsymbol{\alpha})$ is $1 + \mathcal{O}(\epsilon, \delta)$. In view of the preceding definitions $Q(\boldsymbol{\alpha})$ and especially $S(\boldsymbol{\alpha} \to \boldsymbol{\beta})$ we have to specify at which instant in time a CML orbit $\{\mathbf{x}^t, t = 0, 1, 2, \ldots\}$ changes its spin configuration from $\boldsymbol{\alpha}$ to $\boldsymbol{\beta}$. A change $\boldsymbol{\alpha} \to \boldsymbol{\beta}$ is composed out of local transitions/sign changes $\alpha_i, \alpha_{i+1} \to -\alpha_i, \alpha_{i+1}$ as explained in Section 3. For the analysis of a transition we can restrict ourselves to the dynamics of the two neighbouring coordinates x_i^t and x_{i+1}^t. We define the point in time

$t_0 \in \mathbb{N}$ of a transition as the iteration step when the orbit $\{(x_i^t, x_{i+1}^t),\ t = 0, 1, 2, \ldots\}$ of the two coordinates is located in the two dimensional transition set $U^{N=2}(\alpha_i\alpha_{i+1} \to -\alpha_i\alpha_{i+1})$. These transition sets have been introduced in Appendix A: the transition set $U_{-+,++}$ for the type (b) transition $-1, +1 \to +1, +1$ is given in Eq. (A19), the transition set $U_{++,-+}$ for the type (a) transition $+1, +1 \to -1, +1$ in Eq. (A25). The general transition sets $U^{N=2}(\alpha_i\alpha_{i+1} \to \alpha_i\alpha_{i+1})$ for type (a) and (b) transitions can be easily constructed from these examples by symmetry operations. If $(x_i^{t_0}, x_{i+1}^{t_0}) \in U^{N=2}(\alpha_i\alpha_{i+1} \to -\alpha_i\alpha_{i+1})$, it holds $|x_i^{t_0}| \approx 1$, $x_i^{t_0+1} = \mathcal{O}(\epsilon, \delta)$, and in the following iterations the coordinate changes from the interval $J(\alpha_i)$ to $J(-\alpha_i)$. Of course, the definition of the point in time when a transition takes place is to some extent convention.

Concerning Eq. (9) for the transition probability $w(\boldsymbol{\alpha} \mid \boldsymbol{\beta})$, we consider as an example a change of spin configuration $\boldsymbol{\alpha} \to \boldsymbol{\beta}$ with two simultaneous spin flips $\alpha_i, \alpha_{i+1} \to -\alpha_i, \alpha_{i+1}$ and $\alpha_j, \alpha_{j+1} \to -\alpha_j, \alpha_{j+1}$ that are more than one lattice site apart from each other, i.e., $|i-j| > 1$. We now explain that each of the two spin flips contributes a factor $w^{(2)}(\alpha_i\alpha_{i+1} \to -\alpha_i\alpha_{i+1})$ in the transition probability $w(\boldsymbol{\alpha} \mid \boldsymbol{\beta})$. Using the definition of the time of a transition we can write the set $S(\boldsymbol{\alpha} \to \boldsymbol{\beta})$ for the change $\boldsymbol{\alpha} \to \boldsymbol{\beta}$ in leading order perturbation theory

$$S(\boldsymbol{\alpha} \to \boldsymbol{\beta}) \approx U^{N=2}(\alpha_i\alpha_{i+1} \to -\alpha_i\alpha_{i+1}) \times U^{N=2}(\alpha_j\alpha_{j+1} \to -\alpha_j\alpha_{j+1}) \times R \tag{C2}$$

Here the N coordinates are located as follows

$$\begin{aligned}
&(x_i, x_{i+1}) \in U^{N=2}(\alpha_i\alpha_{i+1} \to -\alpha_i\alpha_{i+1}),\\
&(x_j, x_{j+1}) \in U^{N=2}(\alpha_j\alpha_{j+1} \to -\alpha_j\alpha_{j+1}),\\
&(x_1, x_2, \ldots, x_{i-1}, x_{i+2}, \ldots, x_{j-1}, x_{j+2}, \ldots, x_N) \in R.
\end{aligned}$$

The remainder set R has the volume $1 + \mathcal{O}(\epsilon, \delta)$. Using Eq. (C1), the two factors $U^{N=2}(\alpha_i\alpha_{i+1} \to -\alpha_i\alpha_{i+1})$ and $U^{N=2}(\alpha_j\alpha_{j+1} \to -\alpha_j\alpha_{j+1})$ in the direct product in Eq. (C2) give rise to the following factors in the transition probability $w(\boldsymbol{\alpha} \mid \boldsymbol{\beta})$

$$\begin{aligned}
&\mathrm{Area}(U^{N=2}(\alpha_i\alpha_{i+1} \to -\alpha_i\alpha_{i+1})) \cdot \mathrm{Area}(U^{N=2}(\alpha_j\alpha_j \to -\alpha_j\alpha_{j+1}))\\
&\quad = w^{(2)}(\alpha_i\alpha_{i+1} \to -\alpha_i\alpha_{i+1}) \cdot w^{(2)}(\alpha_j\alpha_{j+1} \to -\alpha_j\alpha_{j+1}).
\end{aligned} \tag{C3}$$

For, according to Eqs. (A20) and (A26) the spin flip probabilities are given by the area of the transition set. The generalisation of Eq. (C2) to more than two simultaneous spin flips is straightforward.

If two neighbouring coordinates x_i^t, x_{i+1}^t do not flip at time t_0, we have the condition

$$(x_i^{t_0}, x_{i+1}^{t_0}) \notin U^{N=2}(\alpha_i\alpha_{i+1} \to -\alpha_i\alpha_{i+1}).$$

This gives rise to a factor $(1-w^{(2)}(\alpha_i\alpha_{i+1} \to -\alpha_i\alpha_{i+1}))$ in the transition probability $w(\boldsymbol{\alpha} \mid \boldsymbol{\beta})$.[7]

Now, we would like to show that the canonical distribution of the Ising Hamiltonian is a stationary distribution of the master equation (8) in the approximation of perturbation theory. Hence, we demonstrate that the solution in Eq. (16) satisfies condition (15). For this purpose we analyse the stochastic dynamics of the CML in the "defect picture." The defects on the bonds of the spin chain have been introduced in Section 5. Every change of spin state $\boldsymbol{\alpha} \to \boldsymbol{\beta}$ corresponds to a change of the defect state $\tilde{\boldsymbol{\alpha}} \to \tilde{\boldsymbol{\beta}}$ on the bond lattice. There are four types of local defect processes that have been introduced in the Eqs. (11)–(14). The stationarity condition (15) reads in the defect picture as follows

$$\sum_{\tilde{\gamma} \neq \tilde{\alpha}} w(\tilde{\boldsymbol{\alpha}} \mid \tilde{\gamma}) \cdot p_{\tilde{\gamma}}^{\text{stat}} - \sum_{\tilde{\beta} \neq \tilde{\alpha}} w(\tilde{\boldsymbol{\beta}} \mid \tilde{\boldsymbol{\alpha}}) \cdot p_{\tilde{\alpha}}^{\text{stat}} = 0. \tag{C4}$$

The first term in this equation corresponds to the gain for the defect state $\tilde{\boldsymbol{\alpha}}$, the second term corresponds to the loss out of this state. To solve Eq. (C4) our strategy is to find to each loss term $w(\tilde{\boldsymbol{\beta}} \mid \tilde{\boldsymbol{\alpha}}) \cdot p_{\tilde{\alpha}}^{\text{stat}}$ a corresponding gain term $w(\tilde{\boldsymbol{\alpha}} \mid \tilde{\gamma}) \cdot p_{\tilde{\gamma}}^{\text{stat}}$ that cancels this term.

First, we specify the transition probability of a defect change $\tilde{\boldsymbol{\alpha}} \to \tilde{\boldsymbol{\beta}}$. For large system size N simultaneous defect processes have to be taken into account. The transition probability for a local defect process $\tilde{\alpha}_i, \tilde{\alpha}_{i+1} \to \tilde{\beta}_i, \tilde{\beta}_{i+1}$ that involves two lattice sites in $\tilde{\boldsymbol{\alpha}}$ is given by $\tilde{w}(\tilde{\alpha}_i, \tilde{\alpha}_{i+1})$ (cf. Eqs. (11)–(14)). We can fix the location i of a defect process with the convention that we take the left site of the two sites that are involved in the process. Hence in $\tilde{\boldsymbol{\alpha}} \to \tilde{\boldsymbol{\beta}}$ defect processes of the type i take place at the locations $i \in J_i \subset \{1, 2, \ldots, N\}$. If we define $J := \bigcup_{i=1}^{4} J_i$, at all places $i \in \{1, 2, \ldots, N\} \setminus J$ no defect process takes place. In analogy to Eq. (9) in the "spin picture" the transition probability for $\tilde{\boldsymbol{\alpha}} \to \tilde{\boldsymbol{\beta}}$ reads

$$w(\tilde{\boldsymbol{\beta}} \mid \tilde{\boldsymbol{\alpha}}) = \prod_{i \in J} \tilde{w}(\tilde{\alpha}_i, \tilde{\alpha}_{i+1}) \prod_{i \in \{1, 2, \ldots N\} \setminus J} (1 - \tilde{w}(\tilde{\alpha}_i, \tilde{\alpha}_{i+1})). \tag{C5}$$

[7] In fact, R gives rise to these factors. However, we do not dwell on this highly technical issue here.

For the local transition probabilities $\tilde{w}(\tilde{\alpha}_i, \tilde{\alpha}_{i+1})$ it holds

$$\tilde{w}(\tilde{\alpha}_i, \tilde{\alpha}_{i+1}) \in \{w_k, k = 1, 2, 3, 4\}$$

where w_k denotes the transition probability of the defect process of type k. As explained in Section 5 these probabilities are related to the transition probabilities of the spin flips of type (a) and (b) as follows

$$w_1 = w_2 = w_a, \qquad w_3 = w_4 = w_b. \tag{C6}$$

If no defect process takes place at a lattice site i, we have a factor $(1-\tilde{w}(\tilde{\alpha}_i, \tilde{\alpha}_{i+1}))$ in Eq. (C5).

With Eq. (C5) we can write a loss term in Eq. (C4) as

$$-w(\tilde{\boldsymbol{\beta}} \mid \tilde{\boldsymbol{\alpha}})\, p^{\text{stat}}_{\tilde{\alpha}} = -w_1^{i_1} w_2^{i_2} w_3^{i_3} w_4^{i_4} \prod_{i \in \{1,2,\ldots N\} \setminus J} (1-\tilde{w}(\tilde{\alpha}_i, \tilde{\alpha}_{i+1}))\, p^{\text{stat}}_{\tilde{\alpha}}. \tag{C7}$$

Here i_k denotes the number of elements in the set J_k, i.e., the number of defect processes of type k in $\tilde{\boldsymbol{\alpha}} \to \tilde{\boldsymbol{\beta}}$. It is important to note that in perturbation theory we only have to take changes of defects $\tilde{\boldsymbol{\alpha}} \to \tilde{\boldsymbol{\beta}}$ with

$$i_1 + i_2 + i_3 + i_4 \ll 1 \tag{C8}$$

into account for the master equation (C4). The contribution of $\tilde{\boldsymbol{\alpha}} \to \tilde{\boldsymbol{\beta}}$ with many simultaneous defect processes is strongly suppressed, since each process gives rise a factor of the order $\mathcal{O}(\epsilon, \delta)$ to the transition probability (cf. Eq. (C5)).

We are now going to construct the starting configuration $\tilde{\boldsymbol{\gamma}}$ for the counter process $\tilde{\boldsymbol{\gamma}} \to \tilde{\boldsymbol{\alpha}}$. Figure 9 shows an example of such a construction.

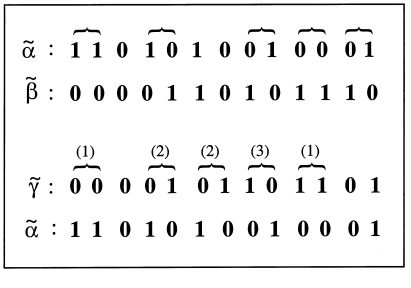

Fig. 9. Here an example of a counter process $\tilde{\boldsymbol{\gamma}} \to \tilde{\boldsymbol{\alpha}}$ to a defect change $\tilde{\boldsymbol{\alpha}} \to \tilde{\boldsymbol{\beta}}$ is shown. The pairs of sites at which defect processes occur are marked by brackets. For the defect state $\tilde{\boldsymbol{\gamma}}$ we also indicate the step number (1), (2) or (3) of the construction. Of course, in the perturbative regime the density of defect processes is much lower than in this figure.

(1) In $\tilde{\gamma} \to \tilde{\alpha}$ the annihilation and creation of two defects is inverted in comparison to the defect change $\tilde{\alpha} \to \tilde{\beta}$. Hence we set

$$\tilde{\gamma}_i = \tilde{\beta}_i, \qquad \tilde{\gamma}_{i+1} = \tilde{\beta}_{i+1}, \qquad \forall i \in J_1 \cup J_4 .$$

(2) We choose i_2 sites i such that $\tilde{\gamma}_i, \tilde{\gamma}_{i+1} \to \tilde{\alpha}_i, \tilde{\alpha}_{i+1}$ is a defect process of type 2 (diffusion to the left).

(3) We choose i_3 sites i such that $\tilde{\gamma}_i, \tilde{\gamma}_{i+1} \to \tilde{\alpha}_i, \tilde{\alpha}_{i+1}$ is a defect process of type 3 (diffusion to the right).

(4) For the remaining sites we set $\tilde{\gamma}_i = \tilde{\alpha}_i$.

Item (2) and (3) are the reason why the configuration $\tilde{\gamma}$ finally differs from $\tilde{\beta}$. To complete the construction the sites mentioned in item (2) and (3) have to be fixed.

For that purpose consider the whole set P of transitions $\tilde{\alpha} \to \tilde{\sigma}$ having a defect process of type 1 (respectively type 4) at $i \in J_1$ (respectively $i \in J_4$) and having i_2 (respectively i_3) processes of type 2 (respectively type 3) at unspecified lattice sites. Our transition under consideration $\tilde{\alpha} \to \tilde{\beta}$ is contained in this set P. On the other hand consider the set Q of counter processes described above, i.e., the set of all processes $\tilde{\tau} \to \tilde{\alpha}$ such that a defect process of type 4 (type 1) occurs at each $i \in J_1$ ($i \in J_4$) and having $i_{2/3}$ defect processes of type 2/3 at unspecified lattice sites. Combinatorics together with the periodic boundary conditions show that P and Q have the same number of elements. Hence we can uniquely assign a counter process to each original process. In particular $\tilde{\gamma} \to \tilde{\alpha}$ can be specified uniquely.

The gain term that results from $\tilde{\gamma} \to \tilde{\alpha}$ in Eq. (C4) is

$$w(\tilde{\alpha} \mid \tilde{\gamma})\, p_{\tilde{\gamma}}^{\text{stat}} = w_1^{i_4} w_2^{i_2} w_3^{i_3} w_4^{i_1} \prod_{i \in \{1,2,\ldots,N\} \setminus K} (1 - \tilde{w}(\tilde{\gamma}_i, \tilde{\gamma}_{i+1}))\, p_{\tilde{\gamma}}^{stat}. \qquad \text{(C9)}$$

Here the set $K \subset \{1, 2, \ldots, N\}$ contains the locations at which local defect processes occur in $\tilde{\gamma} \to \tilde{\alpha}$. The set K has the same cardinality as the set J for the defect change $\tilde{\alpha} \to \tilde{\beta}$.

Now we compare in Eqs. (C7) and (C9) the products of the factors $(1 - \tilde{w}(\tilde{\alpha}_i, \tilde{\alpha}_{i+1}))$ and $(1 - \tilde{w}(\tilde{\gamma}_i, \tilde{\gamma}_{i+1}))$, respectively. One can show from the preceding construction of $\tilde{\gamma}$ that

$$(1 - \tilde{w}(\tilde{\alpha}_i, \tilde{\alpha}_{i+1})) \neq (1 - \tilde{w}(\tilde{\gamma}_i, \tilde{\gamma}_{i+1}))$$

holds at less than $2(i_1 + i_4) + 6(i_2 + i_3)$ lattice sites. Because of condition (C8) that holds in perturbation theory the two products cancel each other approximately, corrections being of order $O(\epsilon^2, \delta^2, \epsilon\delta)$. Besides, the factors

$w_2^{i_2} w_3^{i_3}$ for defect diffusion to the left and right are identical in Eqs. (C7) and (C9). Therefore, we arrive at the condition

$$-w_1^{i_1} w_4^{i_4} p_{\tilde{\alpha}}^{\text{stat}} + w_1^{i_4} w_4^{i_1} p_{\tilde{\gamma}}^{\text{stat}} = 0. \tag{C10}$$

We can solve this condition with the ansatz

$$p_{\tilde{\gamma}}^{stat} = \left(\frac{w_1}{w_4}\right)^{i_1 - i_4} p_{\tilde{\alpha}}^{\text{stat}}.$$

If we compare the number of defects in $\tilde{\boldsymbol{\alpha}}$ and $\tilde{\boldsymbol{\gamma}}$, it holds

$$\#\text{def}(\tilde{\boldsymbol{\alpha}}) - \#\text{def}(\tilde{\boldsymbol{\gamma}}) = 2(i_1 - i_4). \tag{C11}$$

Since the defect state $\tilde{\boldsymbol{\alpha}}$ can be taken arbitrary, we arrive at the following stationary solution of the master equation

$$p_{\tilde{\alpha}}^{\text{stat}} = c \left(\frac{w_1}{w_4}\right)^{-\#\text{def}(\tilde{\alpha})/2} = c \left(\frac{w_b}{w_a}\right)^{\#\text{def}(\tilde{\alpha})/2} \tag{C12}$$

where we have used equation (C6) for the probabilities of defect processes. c is a normalisation constant for the stationary solution. To express the stationary solution in the space of corresponding spin states $\boldsymbol{\alpha}$ we note that

$$\#\text{def}(\tilde{\boldsymbol{\alpha}}) = \tfrac{1}{2} \sum_{i=1}^{N} (\alpha_i \alpha_{i+1} + \tfrac{1}{2}).$$

Therefore the stationary solution for spin states $\boldsymbol{\alpha}$ can be written as

$$p_{\alpha}^{\text{stat}} = c' \left(\frac{w_b}{w_a}\right)^{\sum_{i=1}^{N} \alpha_i \alpha_{i+1}/4} = \frac{1}{Z} \exp\left(\beta J \sum_{i=1}^{N} \alpha_i \alpha_{i+1}\right). \tag{C13}$$

Hence the stationary solution corresponds to the canonical distribution of the nearest neighbour Ising model. For the temperature Eq. (C13) implies

$$\beta J = \frac{1}{4} \ln\left(\frac{w_b}{w_a}\right). \tag{C14}$$

ACKNOWLEDGMENTS

F.S. acknowledges support by the Max-Planck-Institut für Physik komplexer Systeme, Dresden/Germany where main parts of the work were performed.

REFERENCES

1. M. C. Cross and P. C. Hohenberg, *Rev. Mod. Phys.* **65**:851 (1993).
2. B. Schmittmann and R. K. P. Zia, *Statistical Mechanics of Driven Diffusive Systems*, Vol. 17 of *Phase Transitions and Critical Phenomena* (Academic Press, London, 1995).
3. V. Privman, ed., *Non-equilibrium Statistical Mechanics in One Dimension* (Cambridge University Press, 1997).
4. K. Kaneko, ed., *Theory and Applications of Coupled Map Lattices* (Wiley, Chichester, 1993).
5. T. Bohr, M. H. Jensen, G. Paladin, and A. Vulpiani, *Dynamical Systems Approach to Turbulence* (Cambridge University Press, 1998).
6. L. A. Bunimovich and Y. G. Sinai, *Nonlinearity* **1**:491 (1988).
7. J. Bricmont and A. Kupiainen, *Nonlinearity* **8**:379 (1995).
8. F. Schmüser, W. Just, and H. Kantz, *Phys. Rev. E* **61**:3675 (2000).
9. F. Jülicher, A. Ajdari, and J. Prost, *Rev. Mod. Phys.* **69**:1269 (1997)
10. M. O. Magnasco, *Phys. Rev. Lett.* **71**:1477 (1993)
11. D. A. Lavis and G. M. Bell, *Statistical Mechanics of Lattice Systems* (Springer, Berlin, 1999).
12. C. Beck and F. Schlögl, *Thermodynamics of Chaotic Systems* (Cambridge University Press, 1993).
13. P. Gaspard, *Chaos, Scattering and Statistical Mechanics* (Cambridge University Press, 1998).
14. R. Klages and J. R. Dorfman, *Phys. Rev. E* **59**:5361 (1999).